# Transient thermal analysis of semiconductor diode lasers under pulsed operation

G. K. Veerabathran, S. Sprengel, S. Karl, A. Andrejew, H. Schmeiduch, and M.-C. Amann

Citation: AIP Advances **7**, 025208 (2017);
View online: https://doi.org/10.1063/1.4977183
View Table of Contents: http://aip.scitation.org/toc/adv/7/2
Published by the American Institute of Physics

AIP ADVANCES 7, 025208 (2017)

# Transient thermal analysis of semiconductor diode lasers under pulsed operation

G. K. Veerabathran,[a] S. Sprengel, S. Karl, A. Andrejew, H. Schmeiduch, and M.-C. Amann
*Walter Schottky Institut, Technische Universität München, Am Coulombwall 4, 85748 Garching, Germany*

(Received 13 July 2016; accepted 9 February 2017; published online 21 February 2017)

Self-heating in semiconductor lasers is often assumed negligible during pulsed operation, provided the pulses are 'short'. However, there is no consensus on the upper limit of pulse width for a given device to avoid-self heating. In this paper, we present an experimental and theoretical analysis of the effect of pulse width on laser characteristics. First, a measurement method is introduced to study thermal transients of edge-emitting lasers during pulsed operation. This method can also be applied to lasers that do not operate in continuous-wave mode. Secondly, an analytical thermal model is presented which is used to fit the experimental data to extract important parameters for thermal analysis. Although commercial numerical tools are available for such transient analyses, this model is more suitable for parameter extraction due to its analytical nature. Thirdly, to validate this approach, it was used to study a GaSb-based inter-band laser and an InP-based quantum cascade laser (QCL). The maximum pulse-width for less than 5% error in the measured threshold currents was determined to be 200 and 25 ns for the GaSb-based laser and QCL, respectively.  [http://dx.doi.org/10.1063/1.4977183]

## I. INTRODUCTION

Self-heating in semiconductor lasers strongly deteriorates laser characteristics such as threshold current ($I_{th}$), output power and efficiency.[1] This heating is due to non-radiative recombination in the quantum wells (QWs), reabsorption of emitted photons and ohmic losses. Depending on the temperature sensitivity of the gain medium, this hinders proper characterization of the laser. Particularly, in case of mid-infrared laser diodes, the high temperature sensitivity of $I_{th}$ strongly affects all laser parameters during measurements. Principally, self-heating can be overcome by operating the lasers with current pulses short compared to the relevant thermal time constants, instead of continuous wave (CW) operation. However, there is no consensus on the upper limit of pulse width for a given semiconductor laser to avoid self-heating. Values reported in literature typically range between a few tens of *ns* to $\mu s$.[2–4]

Theoretical studies have been reported in the past to determine the thermal transients of laser diodes due to self-heating. Various mathematical models have been developed for diode lasers ranging from simple one-dimensional analysis[5] to more comprehensive models.[6–8] Models based on the electrical equivalence of thermal properties using equivalent electrical circuits have also been proposed.[9,10] However, these theoretical models are not easy to implement in engineering design and many of the parameters used are not easily obtained for some devices. For this reason, several experimental studies have been reported for different laser types. A study was reported on the steady-state heating of quantum cascade lasers (QCLs) in CW operation,[11] however this method can only be used to study lasers that operate in CW mode. Another study measures the average heating of the

[a]Author to whom correspondence should be addressed. Electronic mail: ganpath.veerabathran@wsi.tum.de.

 

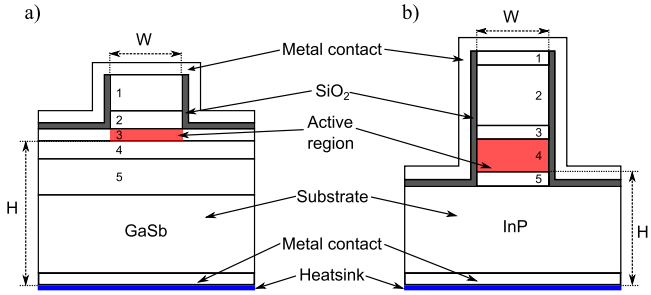


FIG. 1. Schematic cross-section of GaSb-based laser (a) and quantum cascade laser (b). Compositions and thicknesses of the layers are given in Table I. The schematics are not to scale. The electrically pumped part of the active region is highlighted in red. The lasers are processed with ridges of width *W*. *H* is the total thickness of the layers between the active region and heatsink.

active region during pulsed operation as a function of the duty-cycle of the driving current pulses,[12] but this gives no information regarding the transients of the heating. Some methods estimate the thermal transients by detecting the change in terminal voltage,[13] output power[14] or spectral shift during the pulse.[15] Other methods have also been reported using the Michelson interferometer[16] or a high-resolution time-resolved spectroscopy[17] but these methods require specialized equipment, and may be difficult to use on packaged devices.

In this article, we present a measurement technique for transient heat analysis of edge-emitting lasers during pulsed operation. This measurement technique is used to study two types of lasers for different device geometries. Further, a two-dimensional analytical transient thermal model is derived, which is used to extract important parameters for thermal analysis of the lasers from the experimental data.

## II. DEVICE STRUCTURE AND FABRICATION

Two different lasers are analyzed in this paper: a GaSb-based interband laser with type-I quantum wells (QWs) emitting at 3.36 μm and an InP-based injector-less quantum cascade laser (QCL) emitting at 5.7 μm (Details on the lasers are published in ref. 18 and 19 respectively). A schematic cross-section of the processed lasers is shown in Fig. 1(a) for the GaSb laser and Fig. 1(b) for the QCL.

The material compositions and thicknesses of the different layers are listed in Table I. The samples were fabricated into ridge-waveguide lasers. The ridges were defined by reactive ion etching (RIE) after photolithography. In case of the GaSb-based laser, the etching was stopped just before the active region, while the QCL was etched through to the InP- substrate. The sidewalls were then

TABLE I. Composition and layer thicknesses of the two lasers studied. The layer numbers are with reference to the schematic in Fig. 1(a) for the GaSb-based laser and Fig. 1(b) for the QCL.

| Laser | Layer | Material composition | d [μm] |
|---|---|---|---|
| GaSb | 1 | $Al_{0.9}Ga_{0.1}As_{0.08}Sb_{0.92}$ | 3 |
| type-I | 2 | $Al_{0.3}Ga_{0.3}In_{0.4}As_{0.37}Sb_{0.63}$ | 0.3 |
| | 3 | Type-I QWs | 0.07 |
| | 4 | $Al_{0.3}Ga_{0.3}In_{0.4}As_{0.37}Sb_{0.63}$ | 0.3 |
| | 5 | $Al_{0.9}Ga_{0.1}As_{0.08}Sb_{0.92}$ | 3 |
| QCL | 1 | $Ga_{0.4}In_{0.6}As$ | 1 |
| | 2 | $Al_{0.2}Ga_{0.8}As_{0.52}Sb_{0.48}$ | 3.2 |
| | 3 | $Ga_{0.4}In_{0.6}As$ | 0.3 |
| | 4 | QCL active region | 1.6 |
| | 5 | $Ga_{0.4}In_{0.6}As$ | 0.3 |

passivated by sputtering ~200 nm of silicon dioxide for both the laser types. The substrates were thinned chemo-mechanically to ~100 μm, while the stripe widths were 10 and 30 μm. The lasers were then cleaved into different cavity lengths and mounted epi-side up on copper heatsinks with uncoated facets.

## III. MEASUREMENT METHOD

When the temperature of the laser active region increases, it results in a reduction in gain because the injected carriers spread over a wider energy range with higher temperatures. This increases the required carrier densities for threshold resulting in an increased internal loss. The variations of gain and internal loss produce an exponential temperature dependence of $I_{th}$. The relation between $I_{th}$ and temperature can be approximately modeled by:[1]

$$I_{th}(T) = I_{th,ref} \exp\left[\frac{T - T_{ref}}{T_0}\right] \tag{1}$$

where, $I_{th,ref}$ is the threshold current at temperature $T_{ref}$ and $T_0$ is the characteristic temperature, which is a constant.

When a current pulse with sub-threshold amplitude is applied to a laser, the resulting self-heating will increase the temperature of the active volume, thereby increasing $I_{th}$ with time along the pulse. To measure this transience in $I_{th}$, we use two current pulses simultaneously as illustrated in Fig. 2(a). One is the base pulse, $I_B$, with pulse width $\Delta t_B = 8$ μs. $I_B$ is of sub-threshold amplitude and it heats up the laser. The corresponding voltage drop across the laser is $V_B$ and the base pulse power is $q_B$. To probe the transience of $I_{th}$ due to the self-heating induced by $I_B$, we apply a probe current pulse $I_p$, with pulse width $\Delta t_p = 30$ ns, above $I_B$. The temporal position of the probe pulse, $t_p$, is varied along the base pulse and the *P-I* curve of the laser at each $t_p$ is measured by varying only $I_p$ as shown in the inset in Fig. 2(a). This gives the $I_{th}$ of the laser at different times along the base pulse. An illustration of the temperature rise in the active region due to $I_B$ is shown in Fig. 2(b). Figure 3 shows the change in $I_{th}$ with $t_p$ for the GaSb-based laser measured at a constant heatsink temperature, $T_{heatsink} = 25°C$ ('Black' circles). The measured laser has a cavity length of 1 mm and ridge width of 30 μm. The change in $I_{th}$ with $T_{heatsink}$ is also measured for a reference probe pulse position $t_{p,ref} = 0.2$ μs ('Red'

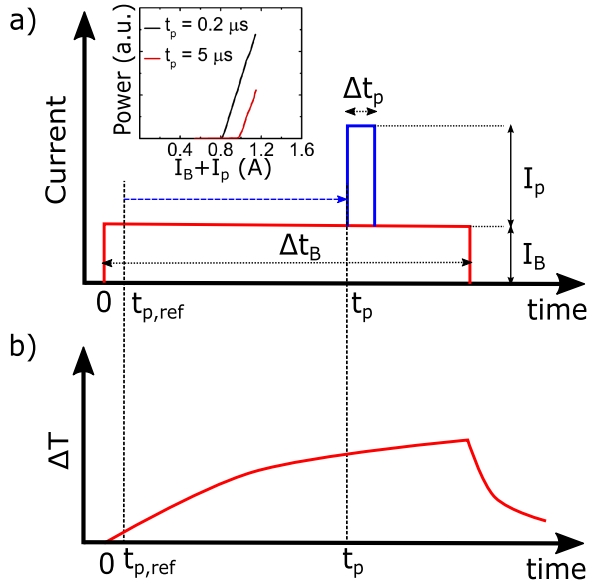


FIG. 2. (a) Schematic of the measurement method with a base pulse $I_B < I_{th}$, which induces self-heating in the laser, and a probe pulse $I_p$ to measure the change in $I_{th}$ along $I_B$. Inset plot shows the *P-I* curves for two different probe pulse positions. (b) Schematic illustration of the relative increase in active region temperature from the moment $I_B$ is applied until it is turned OFF.

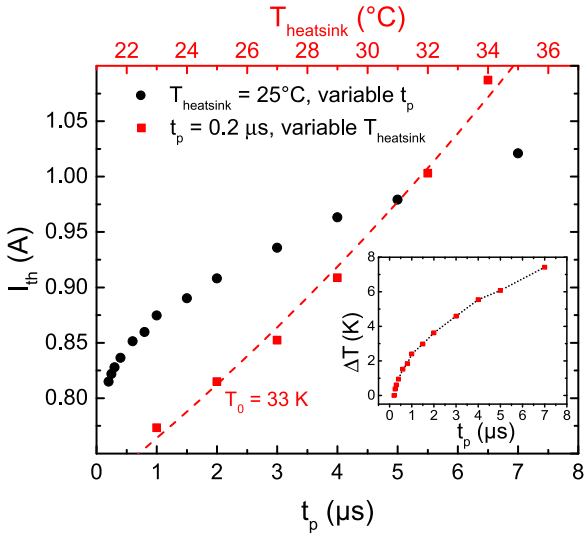


FIG. 3. Variation of $I_{th}$ with time at constant $T_{heatsink}$ ("black" circles) and with $T_{heatsink}$ at constant $t_p$ = 0.2 µs ("red" squares). By correlating these two graphs, the relative change in active region temperature is obtained (see inset graph). From the $I_{th}$ vs. $T_{heatsink}$ curve a $T_0$ of 33 K is extracted for the GaSb laser.

squares in Fig. 3). By correlating these two curves, we extract the relative temperature change in the active region, $\Delta T$, over time by self-heating due to $I_B$, with respect to $t_{p,ref}$ (see inset in Fig. 3).

## IV. ANALYTICAL MODEL

A simplified model of an epi-side up mounted ridge-waveguide laser is considered to obtain an analytical solution for the thermal transients. A schematic cross-section of the model can be seen in Fig. 4(a). Here the thermal conductivity within the laser chip is considered constant and the laser mounted on a perfect heatsink kept at a constant temperature (taken as zero here for convenience). Heat conduction and convection by ambient air is neglected. The heat source is assumed to be concentrated in the active region AB, and is modeled as an infinitely thin stripe of width $W$ with heating power per unit length, $q(t)$ [W/cm]. For an infinitely long pulse which starts at $t = 0$, $q(t)$ can be defined as

$$q(t) = \frac{V_{heat} \times I_{heat}}{L_z} \cdot u(t) \tag{2}$$

where, $V_{heat}$ [V] and $I_{heat}$ [A] are the electrical voltage and current respectively, which heat up the laser, $L_z$ [cm] is the laser cavity length and $u(t)$ is the unit step function. Equation (2) can be

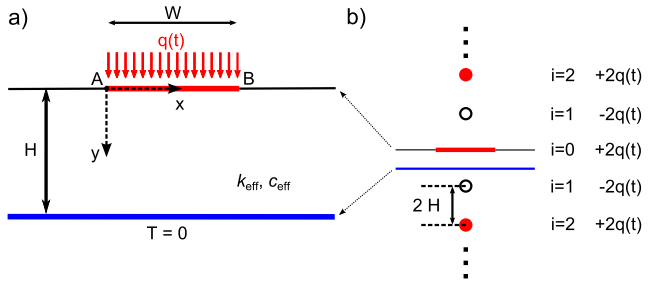


FIG. 4. (a) Schematic of ridge waveguide laser with uniform thermal conductivity and an infinitely thin stripe heat source of width $W$ along AB. An ideal heatsink at $y = H$ has a constant temperature $T = 0$. $k_{eff}$ and $c_{eff}$ are the effective thermal conductivity and volume heat capacitance of the laser. (b) The laser cross-section is mapped onto the $x$-$y$ plane using an infinite set of mirrored heat sources and sinks. The sources and sinks that are away from the active region (AB) are approximated as infinitely thin line sources.

represented as $q(t) = q_{\text{heat}} \cdot u(t)$, where $q_{\text{heat}}$ [W/cm] is the amplitude of the heating pulse. The increase in active region temperature, $\Delta T(t)$, is defined as the average temperature in the active region, *i.e.* along the line AB at $y = 0$.

The laser stripe geometry can be transformed into the entire $x$–$y$ plane using the method of mirror sources and sinks.[20] This automatically satisfies the condition $T = 0$ at $y = H$. The adjacent sources/sinks are separated from each other by $2\ H$, where $H$ is the thickness of the chip. Therefore, the $i^{\text{th}}$ pair of stripe heat source/sink is distanced from the $x = 0$ plane by $2iH$, where $i = 0$ corresponds to the source in AB and $i > 0$ corresponds to the mirror sources/sinks. Considering the ratio of substrate thickness to ridge width, $S = H/W$, for most lasers $S >> 1$ (Also for the lasers studied here (See Sec. II)). Hence, the mirror sources/sinks can be approximated as infinitely thin line sources/sinks as shown in Fig. 4(b). Due to mapping into the upper $x$–$y$ plane, the strengths of the sources and sinks is doubled to $2\ q(t)$ as the heat can flow in both positive and negative $y$-directions.

Considering the contributions of the sources and sinks to $\Delta T(t)$, the stripe source at AB is treated differently to the mirror line sources/sinks. It is treated as a distribution of infinitely thin line sources along AB. Hence, its contribution is obtained by integrating the individual contributions of the line sources to the temperature along line AB and taking the average. However, for the mirror sources/sinks the variations of the temperature contributions along AB is neglected as $S >> 1$. Hence, only their influence at the origin is considered. It must be noted that any point along AB can be chosen for this calculation, however we have taken the point at $x = y = 0$ for convenience. Under these conditions the active region temperature over time for the heat source $q(t)$ is given as (See Appendix A):

$$\Delta T(t) = \left(\frac{q_{heat}}{2\pi k_{eff}}\right)\left(\frac{2\sqrt{\pi}}{\sqrt{\xi}}\right) Erf\left[\sqrt{\xi}\right] + 2E_1\left[\xi\right] + \frac{1}{\xi}\left(E_2\left[\xi\right] - 1\right) + 2\sum_{i=1}^{\infty}(-1)^i E_1\left[\left(\frac{2iH}{W}\right)^2 \xi\right] \tag{3}$$

Here, $\xi = \left(W^2 \middle/ 4D_{eff}t\right)$, where, $D_{eff}$ is the effective thermal diffusivity [cm$^2$/s], which is the ratio of the effective thermal conductivity, $k_{\text{eff}}$ [W/cmK], and the effective volume heat capacity, $c_{\text{eff}}$ [Ws/cm$^3$K]. $Erf$ is the error function and $E_1$ and $E_2$ are exponential integrals. The relevant material parameters are $k_{\text{eff}}$ and $c_{\text{eff}}$. Estimation of these parameters is explained below.

### A. Determination of effective thermal parameters

In the model described above, we made a simplification that the laser chip is composed of a homogeneous material with thermal constants $k_{\text{eff}}$ and $c_{\text{eff}}$. The volume heat capacitances of some semiconductors are listed in Table II. It is evident that this material parameter is similar for most semiconductors, hence an average value of $c_{\text{eff}} = 1.5$ J/cm$^3$K can be used for all lasers. Determination of $k_{\text{eff}}$ is explained below.

The thermal resistance of a substrate of thickness $d$, with a uniform bottom contact and a top contact with stripe geometry of width $W$ and length $L_z$ can be approximated by:[21]

$$R_{th,sub} = \frac{1}{\pi L_z k}\ln\left(\frac{16d}{\pi W}\right) \tag{4}$$

where, $k$ [W/cmK] is the thermal conductivity of the substrate material. Equation (4) is valid for the geometry shown in Fig. 4(a) and it also agrees well with the thermal resistance calculated using

TABLE II. The volume heat capacitances of different semiconductors.[22] Since this material constant is similar for most semiconductors, an average value can be used for $c_{\text{eff}}$ for all the lasers.

| Material | $c_{\text{eff}}$ [J/cm$^3$.K] |
|---|---|
| GaSb | 1.4 |
| InP | 1.49 |
| GaAs | 1.76 |
| InAs | 1.42 |
| Si | 1.63 |

TABLE III. The effective thermal conductivities of the lasers analyzed in this paper. $k_{\text{eff}}$ depends on the geometry and material parameters of the different layers in the laser.

| Laser type | Ridge width [μm] | $k_{\text{eff}}$ [W/cm.K] |
|---|---|---|
| GaSb type-I | 10 | 0.14 |
| | 30 | 0.2 |
| QCL | 30 | 0.37 |

Eq. (3), given by $R_{th,sub} = \Delta T(t \to \infty)/(q_{heat}L_z)$, taking $k_{\text{eff}} = k$ ($c_{\text{eff}}$ has no influence on the steady-state conditions).

The thermal resistance of the active region with the heat source distributed over the entire volume, thickness $d_{\text{AR}}$, thermal conductivity $k_{\text{AR}}$, ridge width $W$ and length $L_z$ is given by (See Appendix B):

$$R_{th,AR} = \frac{1}{k_{AR}} \frac{(d_{AR}/3)}{WL_z} \tag{5}$$

This is the same as the thermal resistance of a cuboid with one-dimensional heat flow, where the heat-source is concentrated in the upper interface and with an effective layer thickness which is one third of the actual value. Here, heat conduction in the active region is considered one-dimensional, which is valid only for the cases where its thickness is negligible compared to the mesa width or it is etched through. Therefore, this model cannot be applied to lasers where lateral heat conduction in the active region plays a non-negligible role. For example, it cannot be used on buried hetero-structure lasers[23] or even ridge waveguide lasers with thick electroplated gold on top for improved lateral heat extraction.[24] From Eq. (4) and (5), the thermal resistance of the ridge-waveguide lasers shown in Fig. 1 is approximated as:

$$R_{th} = \frac{1}{WL_z}\left(\frac{(d_{AR}/3)}{k_{AR}} + \sum_{n=1}^{N}\frac{d_n}{k_{th,n}}\right) + \frac{1}{\pi L_z k_{th,sub}} \ln\left(\frac{16d_s}{\pi W}\right) \tag{6}$$

where, $d_{\text{n}}$ is the thickness and $k_{\text{th,n}}$ is the thermal conductivity of the $n^{\text{th}}$ layer below the active region and $d_{\text{s}}$ and $k_{\text{th,s}}$ are the thickness and thermal conductivity of the substrate respectively. Here, heat conduction through the layers above the active region is ignored as heat is assumed to flow only downwards to the heatsink. In addition, lateral heat conduction in all the layers except the substrate is neglected as $d_{\text{AR,n}} << d_{\text{s}}$. With $R_{\text{th}}$ from Eq. (6), we can calculate the $k_{\text{eff}}$ for which we have the same thermal resistance for the model in Fig. 4(a) using Eq. (4). This reads:

$$k_{eff} = \frac{\ln\left(16H/\pi W\right)}{\frac{\pi}{W}\left(\frac{(d_{AR}/3)}{k_{AR}} + \sum_{n=1}^{N}\frac{d_n}{k_{th,sub}}\right) + \frac{1}{k_{th,sub}} \ln\left(\frac{16d_s}{\pi W}\right)} \tag{7}$$

where, $H = (d_{AR}/3) + \sum_{n=1}^{N} d_n + d_s$. It can be seen in Eq. (7) that $k_{\text{eff}}$ is independent of $L_{\text{z}}$, however, it depends on $W$, $d_{\text{AR}}$, $d_{\text{n}}$ and $d_{\text{s}}$ in addition to the thermal conductivities of the materials. Therefore, it depends on the geometry and material parameters of the different layers in the laser. In Table III, the $k_{\text{eff}}$ for the different lasers studied in this paper are listed. The thermal conductivities of the materials used in calculating $k_{\text{eff}}$ were taken from the literature.[25,26] It can be noted that the QCL has a higher $k_{\text{eff}}$ compared to the GaSb laser, as InP has nearly twice the thermal conductivity compared to GaSb.

## V. RESULTS AND DISCUSSION

Here we present the temperature transience of the active region ($\Delta T$) of two different laser types due to self-heating during pulsed operation. The $\Delta T$ is experimentally determined using the method

described in Sec. III for the two laser types. For both lasers, the effect of change in cavity length ($L_z$) is studied. For the GaSb-based laser, additionally, $W$ is varied for the same $L_z$. The measurement data ('Black' squares and 'green' triangles) is shown in Figures 5 and 6. For all these measurements $t_{p,ref}$ = 0.2 μs (see Sec. III). Table IV shows the details of the lasers along with the measured $I_B$ and $V_B$. Although, $I_B = I_{heat}$ always, not all of $V_B$ goes into heating the laser. Some of the voltage drop occurs far enough from the active region to have no influence on $\Delta T$. Therefore, to determine the actual heating power, $q_{heat}$, the thermal transients of the lasers are numerically simulated using COMSOL Multiphysics.[27] The schematics of the simulation models are the same as in Fig. 2. Thermal conductivity, specific heat and mass density of the different materials shown Table I are taken from the literature.[22,25,26,28,29] The heat source is assumed concentrated in the active regions of the lasers, which are highlighted in Fig. 1, and the heat is assumed to flow downward to a perfect heat sink below the substrate. Heat transfer by conduction or convection by the ambient air is neglected. The actual heating power is obtained by fitting the numerical simulation to the measurement data using $q_{heat}$ as the fitting parameter. The simulation results are also shown in Figures 5 and 6 ('Red' dashed curves). The resulting values of $q_{heat}$ and the corresponding $V_{heat}$ are listed in Table IV. Finally, $\Delta T$ is calculated using Eq. (2), by plugging in the effective thermal parameters from Sec. IV and $q_{heat}$ from

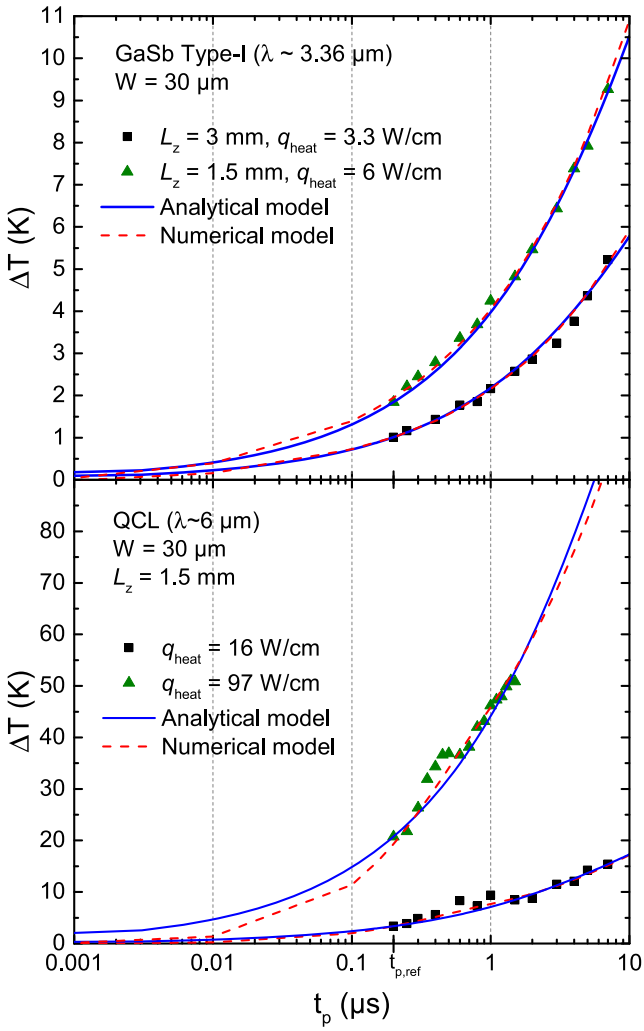


FIG. 5. Increase in active region temperature of 30 μm ridges of the two laser types for different heating powers per unit length. The measurement points are given an offset to match the temperature from the analytical model at $t_{p,ref}$ = 0.2 μs. The measurement (squares and triangles) agrees well with the numerical (dashed red lines) and analytical models (solid blue lines). The self-heating before $t_{p,ref}$ is estimated using the analytical and numerical models.

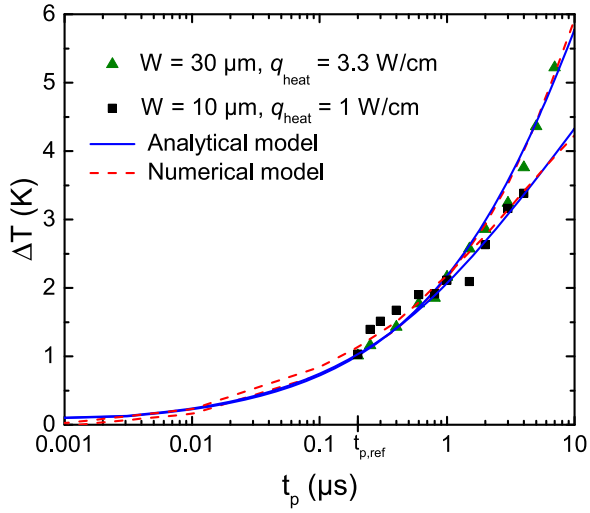


FIG. 6. Increase in active region temperature of GaSb lasers with cavity length of 3 mm and different ridge widths. The measurement points are given an offset to match the temperature from the analytical model at $t_{p,ref}$. The smaller ridge width has lower self-heating due to a lower $q_{heat}$.

Table IV. The results of the analytical model ('Blue' solid curves) are also plotted in Figures 5 and 6 along with the measurement data and numerical simulations and they show excellent agreement. The normalized root-mean-square (RMS) deviation of the model to experimental data, normalized to the range of the experimental data, is less than 10%.

The effect of cavity length on the self-heating of the lasers with W = 30 μm, can be seen in Fig. 5 for the GaSb laser and the QCL. In general, for Fabry Perot lasers with the same $W$, those with smaller $L_z$ have more self-heating. It must be noted that heat-dissipation in the edge-emitting laser is two dimensional phenomenon and length doesn't play a role. However, lasers with smaller $L_z$ have higher mirror losses, resulting in higher threshold current densities and hence higher $q_{heat}$.[30] This is evident from the $\Delta T$ of the two GaSb lasers in Fig. 5, wherein, the shorter laser heats up more due to a higher $q_{heat}$. Despite having higher $k_{eff}$ compared to the GaSb laser (see Table III), the QCL has much higher self-heating due to its larger $q_{heat}$. Figure 6 shows the effect of variation of $W$ (10 and 30 μm) for $L_z$ = 3 mm, for the GaSb laser. Even though the thermal resistance of the laser is smaller for larger $W$ (see Eq. (6)), the laser with the wider ridge has more self-heating because $q_{heat}$ scales more rapidly with $W$ than the resistance goes down.

### A. Determination of proper pulse width for laser characterization

Using the analytical model, thermal transients before $t_{p,ref}$ can also be estimated, as shown in Fig. 5 and Fig. 6. This information is critical to determine the proper pulse width, $\Delta t_{pulse}$, for laser characterization to limit measurement error due to self-heating. The error in the measurement of $I_{th}$

TABLE IV. Cavity length ($L$), applied base pulse current ($I_B$) and measured voltage drop across the lasers ($V_B$). The actual heating power per unit length $q_{heat}$ and the corresponding voltage $V_{heat}$ obtained from numerical simulations are also listed.

| | | | Measurement | | Simulation | |
|---|---|---|---|---|---|---|
| Laser | $L$ [mm] | Ridge width [μm] | $I_B$ [A] | $V_B$ [V] | $V_{heat}$ [V] | $q_{heat}$ [W/cm] |
| GaSb type-I | 1 | 30 | 0.55 | 2.8 | 1.1 | 6 |
| | 3 | 30 | 0.83 | 3 | 1.18 | 3.3 |
| | 3 | 10 | 0.35 | 2.6 | 0.85 | 1 |
| QCL | 1.5 | 30 | 0.26 | 12.2 | 9 | 16 |
| | 1.5 | 30 | 1.16 | 15.5 | 12.5 | 97 |

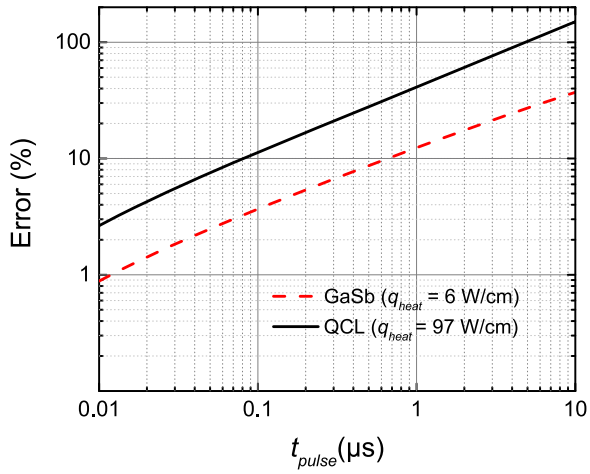


FIG. 7. Error in percentage of the measured threshold current in pulsed mode as a function of pulse width for a GaSb-based laser and QCL, both with a ridge width of 30 μm.

as a function of $\Delta t_{\text{pulse}}$ for a certain $q_{\text{heat}}$ is defined as:

$$Error(\Delta t_{pulse}) = \frac{I_{th}(\Delta t_{pulse}) - I_{th}(\Delta t_{pulse} \to 0)}{I_{th}(\Delta t_{pulse} \to 0)} \tag{8}$$

Using Eq. (7), Eq. (8) can be simplified to:

$$Error(\Delta t_{pulse}) = \left(\exp\left[\frac{\Delta T(\Delta t_{pulse})}{T_0}\right] - 1\right) \tag{9}$$

Error in percentage plotted against $\Delta t_{\text{pulse}}$ for a GaSb laser and a QCL is shown in Fig. 7. The $T_0$ of the GaSb laser is 33 K (see Fig. 3) while that of the QCL is 120 K.[19] From Fig. 7 it can be seen that for an error tolerance of 5%, the maximum $\Delta t_{\text{pulse}}$ for the GaSb laser is ~200 ns, while for the QCL it is ~25 ns. Despite having very good temperature stability in the active region (high $T_0$) the QCL has a lower tolerance in the allowed pulse widths due to the much higher $q_{\text{heat}}$. The maximum $\Delta t_{\text{pulse}}$ for pulsed characterization for a laser depends on various parameters such as the thermal properties of its materials, geometry, $q_{\text{heat}}$ and the tolerance in the error required. Using the model and Eq. 9, the maximum $\Delta t_{\text{pulse}}$ for negligible self-heating effects can be estimated.

## VI. CONCLUSION

In this paper we presented an experimental method to measure the transient heating of edge-emitting semiconductor lasers. It is based on the change in the threshold current of the laser over time due to self-heating during pulsed operation. So it can be used to directly measure the transience of the mean active region temperature during the pulse. Owing to its generality, it can be applied to all kinds of edge-emitting lasers to study their thermal transients, which will be highly beneficial for the optimization of their thermal design. Importantly, it can be used to study lasers which do not operate in continuous-wave mode.

Additionally, we developed a two dimensional analytical model describing transient heat dissipation in ridge waveguide semiconductor lasers. With material parameters, device geometry and heating power as input, the model can be used to calculate the thermal transients of most edge-emitting devices. Due to the approximations made in the model, it is applicable only to lasers with stripe width much smaller than the substrate thickness and with negligible lateral heat conduction in the active region. This analytical model when used in conjunction with experimental data, can be used to extract important parameters required for transient thermal analysis of lasers. Another application is the determination of measurement parameters for negligible self-heating effects, such as the upper limit for the pulse width during pulsed characterization of lasers.

To validate the presented approach for transient thermal analysis, a GaSb based laser and a QCL were studied. The experimental data, analytical model and numerical simulation using COMSOL show excellent agreement. Further, the analytical model was used to determine the upper limit of the pulse width for less than 5% error in the measured threshold current due to self-heating of the lasers during the pulse.

## ACKNOWLEDGMENTS

This work was supported by the excellence cluster "Nano-initiative Munich" (NIM) and by the German Research Foundation (DFG) and the Technical University of Munich (TUM) in the framework of the Open Access Publishing Program.

## APPENDIX A: DERIVATION OF ΔT(t)

In this appendix, we derive Eq. (3) as a solution to the problem described in Sec. IV. The differential equation for the temperature distribution due to an infinitely thin line source at the origin in Fig. 4(a) is given by:

$$\frac{\partial T(x,y,t)}{\partial t} = D_{eff}\nabla^2 T(x,y,t) + \frac{q(t)}{c_{eff}}\delta(y)(u(x) - u(x-W)) \tag{A1}$$

where, $q(t)$ is the time-dependent heat-source power per unit length [W/cm]. $\delta$ and $u$ are the delta and unit step functions respectively. For a $\delta$-pulse at $t = 0$, $q(t) = q_{\text{heat}}{\cdot}\delta(t)$, where $q_{\text{heat}}$ is the heat per unit length, and the corresponding solution to Eq. (A1) reads:[31]

$$T_\delta(x,y,t) = \frac{2q_{heat}}{4\pi k_{eff}\, t}\exp\left(-\frac{x^2+y^2}{4D_{eff}\, t}\right) \tag{A2}$$

where, the factor of two stems from the doubling of the source strength due to mapping (See Fig. 4(b)). The effect of a step heat source at $t = 0$ at the origin given by $q(t) = q_{\text{heat}}{\cdot}u(t)$, can be obtained by integrating Eq. (A2) over time, yielding:

$$T_u(x,y,t) = \frac{2q_{heat}}{4\pi k_{eff}}\int_0^t \frac{1}{t'}\exp\left(-\frac{x^2+y^2}{4D_{eff}\, t'}\right)dt' \tag{A3}$$

In the model shown in Fig. 4 (a), there is a distribution of line sources along the line AB with heat flux density $q_{\text{heat}}/W$ [W/cm$^2$]. Summing the contribution of these line sources and averaging the temperature along AB gives:

$$T_{AV}(t) = \frac{2q_{heat}}{4\pi k_{eff} W}\int_0^t\int_0^W \frac{1}{W}\int_0^W \frac{1}{t'}\exp\left(-\frac{(x-x')^2}{4D_{eff}\, t'}\right)dx'dxdt' \tag{A4}$$

The contribution of the mirror sources and sinks shown in Fig. 4(b) is obtained by neglecting the variations of the temperature contributions along the stripe AB (since $H >> W$). The contributions of the sources and sinks is considered only at the origin for convenience. This yields for the sources and sinks,

$$T_i(t) = \frac{2q_{heat}}{4\pi k_{eff} W}\int_0^t\int_0^W \frac{1}{t'}\exp\left(-\frac{(2iH)^2}{4D_{eff}\, t}\right)dx'dt' \tag{A5}$$

where, $2iH$ is the distance of the source/sink $i$ ($i = 1, 2, \ldots$) from the origin. The total time dependent increase in temperature of the stripe AB or the active region is obtained by summing the contribution of all the sources and sinks, yielding:

$$\Delta T(t) = T_{AV}(t) + 2\sum_{i=1}^{\infty}(-1)^i T_i(t) \tag{A6}$$

where, the factor $(-1)^i$ determines if the contribution is from a source (even indices) or a sink (odd indices). Completing the integrals in Eq. (A6) yields Eq. (3).

## APPENDIX B: THERMAL RESISTANCE OF THE ACTIVE REGION

In this appendix, the thermal resistance of the active volume of the lasers, which are highlighted in Fig. 1, is derived. As the thickness of the active volume is negligible compared to the substrate thickness, heat transfer is assumed to be one-dimensional. The active volume has a thickness of $d_{\mathrm{AR}}$, thermal conductivity $k_{\mathrm{AR}}$ and heat source per unit volume of $\alpha$ W/cm$^3$. The differential equation governing the steady-state heat transfer in the active volume is given by:

$$\frac{d^2T(y)}{dy^2} = -\frac{\alpha}{k_{AR}} \tag{B1}$$

The heat flux is assumed to flow only downward to the heatsink. Integrating Eq. (B1) twice and applying the boundary conditions $T'(y=0)=0$ and $T(y=d_{\mathrm{AR}})=0$, we get the solution to Eq. (B1):

$$T(y) = \frac{\alpha}{2k_{AR}}(d_{AR}^2 - y^2) \tag{B2}$$

The average active region temperature is obtained by integrating Eq. (B2) over the entire thickness and dividing by it, giving:

$$T_{AR} = \frac{\alpha d_{AR}^2}{3k_{AR}} \tag{B3}$$

The thermal resistance of the active region, $R_{\mathrm{th,AR}}$, is obtained by differentiating $T_{\mathrm{AR}}$ by the total heating power $P$. Substituting $\alpha = P/(W\,L_z\,d_{\mathrm{AR}})$ in Eq. (B3) and differentiating by $P$ gives Eq. (5).


[1] J. Pankove, IEEE J. Quantum Electron **4**, 119 (1968).
[2] R. Weih, A. Bauer, M. Kamp, and S. Höfling, Opt. Mater. Express **3**, 1624 (2013).
[3] L. Li, Y. Jiang, H. Ye, R. Q. Yang, T. D. Mishima, M. B. Santos, and M. B. Johnson, Appl. Phys. Lett. **106**, 251102 (2015).
[4] V. Spagnolo, G. Scamarcio, H. Page, and C. Sirtori, Appl. Phys. Lett. **84**, 3690 (2004).
[5] W. Engeler and M. Garfinkel, Solid State Electron **8**, 585 (1965).
[6] C. A. Evans, V. D. Jovanovic, D. Indjin, Z. Ikonic, and P. Harrison, IEEE J. Quantum Electron **42**, 859 (2006).
[7] S. C. Chaparala, F. Xie, C. Caneau, C. E. Zah, and L. C. Hughes, IEEE Trans. Compon. Packag. Manuf. Technol. **1**, 1975 (2011).
[8] W. B. Joyce and R. W. Dixon, J. Appl. Phys. **46**, 855 (1975).
[9] P. S. André, P. Antunes, A. L. J. Teixeira, and J. L. Pinto, Las. Phys. Lett. **2**, 525 (2005).
[10] Q. Shan, Q. Dai, S. Chhajed, J. Cho, and E. F. Schubert, J. Appl. Phys. **108**, 084504 (2010).
[11] J. Faist, F. Capasso, C. Sirtori, D. L. Sivco, A. L. Hutchinson, and A. Y. Cho, Appl. Phys. Lett. **67**, 3057 (1995).
[12] M. Wienold, M. P. Semtsiv, I. Bayrakli, W. T. Masselink, M. Ziegler, K. Kennedy, and R. Hogg, J. Appl. Phys. **103**, 083113 (2008).
[13] H.-Y. Ryu, K.-H. Ha, J.-H. Chae, O.-K. Nam, and Y.-J. Park, Appl. Phys. Lett. **87**, 093506 (2005).
[14] H. I. Abdelkader, H. H. Hausien, and J. D. Martin, Rev. Sci. Instrum. **63**, 2004 (1992).
[15] R. L. Tober, J. Appl. Phys. **101**, 044507 (2007).
[16] M. Suyama, N. Ogasawara, and R. Ito, Jpn. J. Appl. Phys. **20**, L395 (1981).
[17] W. G. Scheibenzuber and U. T. Schwarz, Appl. Phys. Lett. **98**, 181110 (2011).
[18] K. Vizbaras, A. Vizbaras, A. Andrejew, C. Grasse, S. Sprengel, and M.-C. Amann, Proc. SPIE **8277**, 82771B (2012).
[19] S. Katz, A. Vizbaras, G. Boehm, and M.-C. Amann, Appl. Phys. Lett. **94**, 151106 (2009).
[20] H. Carslaw and J. Jaeger, *Conduction of Heat in Solids* (Oxford, U.K., Clarendon, 1990), Sec. 10.10.
[21] M.-C. Amann, Appl. Phys. Lett. **50**, 4 (1987).
[22] *Handbook Series on Semiconductor Parameters* – Vol. 1, edited by M. Levinshtein, S. Rumyantsev, and M. Shur (World Scientific, Singapore, 1996).
[23] M. Beck, J. Faist, U. Oesterle, M. Ilegems, E. Gini, and H. Melchior, IEEE Photon. Technol. Lett. **12**, 1450 (2000).
[24] J. S. Yu, S. Slivken, A. Evans, L. Doris, and M. Razeghi, Appl. Phys. Lett. **83**, 2503 (2003).
[25] S. Adachi, J. Appl. Phys. **102**, 063502 (2007).
[26] A. Lops, V. Spagnolo, and G. Scamarcio, J. Appl. Phys. **100**, 043109 (2006).
[27] COMSOL Multiphysics® v. 5.2. www.comsol.com COMSOL AB, Stockholm, Sweden.
[28] S. Andersson and L. Dzhavadov, J. Phys.: Condensed Matter **4**, 6209 (1992).
[29] *American Institute of Physics Handbook*, edited by D. E. Gray (McGraw-Hill, New York, 1972), Table 4g–8.
[30] A. Kurobe, H. Furuyama, S. Naritsuka, N. Sugiyama, Y. Kokubun, and M. Nakamura, IEEE J. Quantum Electron **24**, 635 (1988).
[31] A. V. Luikov, *Analytical heat diffusion theory* (Academic Press, New York, 1968).